Collective director modes at the transitions to hexatic ferroelectric liquid crystalline phases

J. Schacht, F. Gießelmann, and P. Zugenmaier

Institute of Physical Chemistry, Technical University of Clausthal, Arnold-Sommerfeld-Strasse 4, D-38678 Clausthal-Zellerfeld, Germany

W. Kuczyński

Institute of Molecular Physics, Polish Academy of Sciences, Smoluchowskiego 17, 60-179 Poznań, Poland

(Received 21 October 1996)

Measurements of the dielectric constant and the modulation depth of the light intensity as a function of temperature and electric field frequency are reported for two compounds of the homologous series 4-[(S)-2-chloro-3-methylbutanoyloxy]-4'-[4-n-alkyloxybenzoyloxy]biphenyl exhibiting cholesteric, smectic-A^*, smectic-C^*, hexatic-I^*, and hexatic-F^* phases. Relaxation processes related to the hexatic-I^*–smectic-C^* and hexatic-to-hexatic phase transitions are characterized and the results discussed in terms of bond orientational order and its coupling to the molecular tilt direction. Parameters describing this coupling are determined by fitting the results of a theoretical model to the experimental data. [S1063-651X(97)04905-2]

PACS number(s): 64.70.Md, 77.84.Nh, 78.20.Jq

I. INTRODUCTION

Landau [1] and Peierls [2] independently established that a periodic lattice cannot exist in a one- or two-dimensional system. Landau [3] also realized that the vectors describing the relative positions of the center of mass of particles can form long range orientational order, which leads to anisotropy in these systems without long range positional order. This kind of order has been termed long range bond orientational order. Some smectic liquid crystalline phases exhibit this long range bond orientational order [4], but they lack long range positional order within smectic layers or between them, e.g., hexatic smectic phases [5]: Sm-B_{hex}, Sm-I, Sm-F. Meyer *et al.* [6] pointed out that the chiral tilted hexatic phases (Sm-I^*, Sm-F^*) should exhibit pyroelectric properties similar to the smectic-C^* phase (Sm-C^*). This gives rise to a macroscopic spontaneous polarization and a ferroelectric domain structure, if they are prepared in sufficiently thin cells (surface stabilized ferroelectric liquid crystal, SSFLC [7]) or if a large electric or magnetic field is applied.

The structure of hexatic, smectic phases has been analyzed using x-ray scattering techniques [8–11]. Heat capacity measurements are suitable for investigations of various phase transitions [12–16], also in free standing films [17]. In the vicinity of phase transitions in smectics, the dynamical properties of chiral and nonchiral hexatic phases have been investigated by light scattering techniques [18–22]. Dierker and Pindak [18], Nelson and Halperin [23], and Selinger and Nelson [24,25] proposed a theory which describes hexatic-to-hexatic phase transitions.

In materials with high spontaneous polarization ($P_s > 200$ nC cm^{-2}), the nature of hexatic-to-hexatic phase transitions is appropriately probed by dielectric spectroscopy or electro-optical methods, where reorientations of the spatial director structure can be monitored as optical transmission signals. Dielectric investigations concerning the transitions from Sm-C^* to chiral tilted hexatic phases are rare [26], however.

In this paper we report results of dielectric measurements in the cholesteric and different tilted smectic phases, e.g., fluid Sm-C^* and hexatic Sm-I^* and Sm-F^* phases and compare them to those by an optical method. Both are discussed in terms of the evolution of the bond orientational order, the local tilt direction, and their coupling. Following the ideas of Selinger and Nelson [24], the coupling between the spatially fixed long range bond orientational order and the local tilt direction becomes weak in the vicinity of the Sm-F^*–Sm-I^* phase transition, therefore a reorientation of the local tilt direction with respect to the bond orientational order is caused by the strong interaction between the large spontaneous polarization and an electric field. A new collective director mode is related to this reorientation.

II. EXPERIMENT

Two members of series Mn with its general chemical formula given below exhibit Sm-C^* and hexatic smectic phases on cooling.
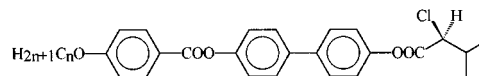
Their synthesis has been described elsewhere [27] and chiral properties of compounds Mn with $3 \leq n \leq 10$ have been reported in a previous paper [28]. In this work, the molecular dynamics of different ferroelectric phases are studied in compounds $M6$ and $M10$. Two types of sample geometry different in alignment of smectic layers with respect to the substrates are schematically depicted in Fig. 1 and referred to as (a) ''planar orientation'' and (b) ''homeotropic orientation,'' respectively.

(a) Commercially available SSFLC cells (E.H.C. Ltd., Tokyo, indium tin oxide (ITO) electrode area 1 cm^2, parallel rubbed polyimide coatings, 10 μm cell gap) are filled by capillary action in the cholesteric phase. These samples exhibit a nearly perfect Grandjean [29] texture in the cholesteric phase with its helical axis aligned perpendicular to the substrates. In the Sm-C^* phase, compounds Mn exhibit a distorted helical structure with the helical axis aligned nearly parallel to the substrates as inferred from the observation of distinct, equally spaced disclination lines. Polar anchoring of
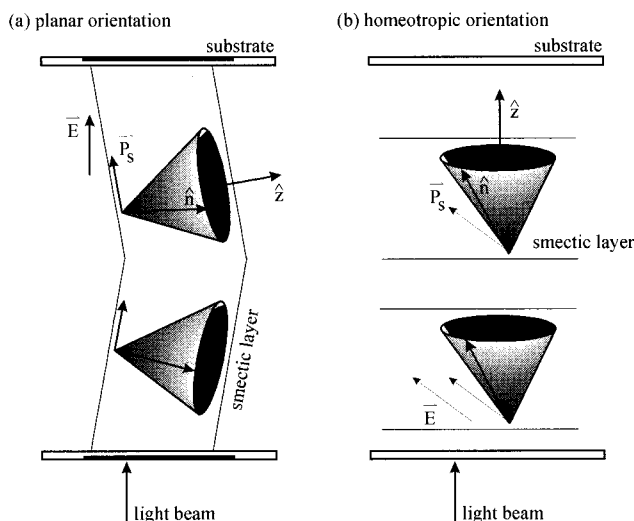
FIG. 1. Principal geometries of samples: (a) the ''planar orientation'' in SSFLC cells, (b) ''homeotropic orientation'' obtained by unidirectional shearing.

molecules at the substrates stabilizes a pretilt [30] and smectic layers form a chevron structure [31].

(b) Strong, unidirectional shearing in the Sm-C^* phase forces the smectic layers to align parallel to the substrates of a homemade liquid crystal (LC) cell with a cell gap of less than 1 μm being composed of two untreated glass plates. One of the glass plates carries two parallel metal electrodes with a distance of 1 mm, hence the electric field is applied parallel to the smectic layers (''homeotropic orientation'' or ''in plane switching geometry''). The tilt direction is aligned nearly parallel to the direction of shearing and a strongly deformed Sm-C^* helicoidal structure is formed.

All samples are placed in a modified Mettler model no. FP52 hot stage equipped with a temperature controlling unit (Unipan 650H). The temperature is controlled within 0.02 K, the absolute temperature calibration within ± 1 K, respectively. Electric field induced distortions of the spatial director structure are recorded using two methods, (i) the dielectric and (ii) an electro-optical method, respectively, and depicted schematically in Fig. 2.

(i) The low frequency (LF) impedance analyzer model no. HP4192A is used in combination with a computer controlled setup for measuring the complex dielectric permittivity $\varepsilon^* = \varepsilon' - i\varepsilon''$ as a function of temperature and frequency. The electrode area in a sample prepared in ''homeotropic orientation'' is very small, the dielectric method is not applicable here.
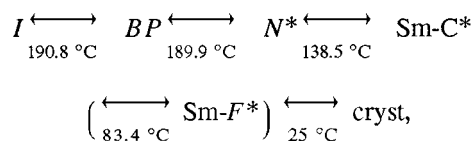
(ii) Both types of samples are placed in a polarizing microscope. The application of an electric field causes a small modulation in the intensity of transmission of visible light (546 nm). The depth of modulation is detected by a photodiode as a function of temperature and frequency of the electric field applied. After preamplification, the signal is transferred to a lock-in amplifier (Stanford Research Systems SR 530), which is synchronized by the ac voltage applied to the cells (HP 4192A for SSFLC cells or function generator Zopan KF140S and power generator Zopan P0-27 for homemade cells, which stabilizes a ''homeotropic orientation''). Output signals are accumulated (256 times) and averaged by the HP 54602A oscilloscope connected to a computer for data storage.

For both types of samples, the driving voltage is chosen as low as possible (10 mV per micrometer) in order to prevent any irreversible distortion of the spatial director structure. A comparison between the electro-optic and the dielectric method, a discussion of their advantages, and details of the setup are summarized elsewhere [35].

III. RESULTS AND DISCUSSION

Dielectric measurements for compound $M6$ are reported and discussed in the first part of this section with special attention to temperature regions near the phase transitions. These results are compared with those obtained by the electro-optical method and discussed in terms of collective director modes related to the phase transitions (e.g., Sm-C^*–Sm-F^*). In the second part, measurements in the vicinity of a hexatic-to-hexatic phase transition of compound $M10$ are described in terms of the bond orientational order and the local tilt direction ($\vec{c}$ director) in hexatic smectics. In an electric field, the coupling between both directions is disturbed by the $\vec{P}_s \cdot \vec{E}$ interaction, which has to be added to the free energy density expansion.

Compound $M6$ exhibits the following phase sequence on cooling:

$$I \underset{190.8\,°C}{\overset{\longleftrightarrow}{}} BP \underset{189.9\,°C}{\overset{\longleftrightarrow}{}} N^* \underset{138.5\,°C}{\overset{\longleftrightarrow}{}} \text{Sm-C}^*$$

$$\left(\underset{83.4\,°C}{\overset{\longleftrightarrow}{}} \text{Sm-}F^* \right) \underset{25\,°C}{\overset{\longleftrightarrow}{}} \text{cryst},$$

where the parentheses denote the monotropic phase (cf. caption to Fig. 3). The dielectric permittivity is determined in cells with a ''planar orientation.'' The dielectric constant $\varepsilon'(T)$ at a fixed oscillator frequency of 200 kHz is depicted in Fig. 3. Generally, the values of ε' increase on approach-
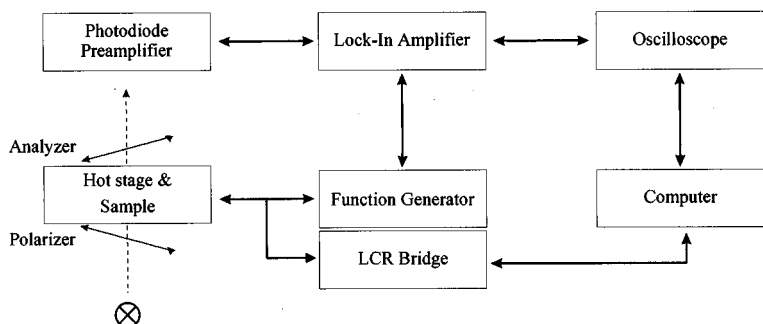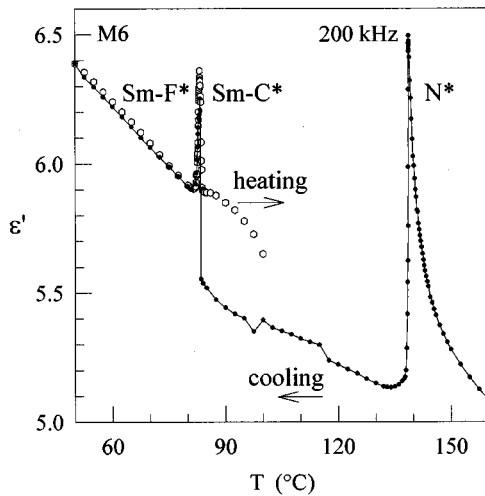

FIG. 2. Experimental setup.

FIG. 3. Dielectric constant ε' versus temperature for compound $M6$ at 200 kHz in the ''planar orientation.'' A hysteresis in the Sm-C^* phase is observed between cooling and heating. (Crystallization of $M6$ must be avoided since the Sm-F^* phase is a monotropic phase.)
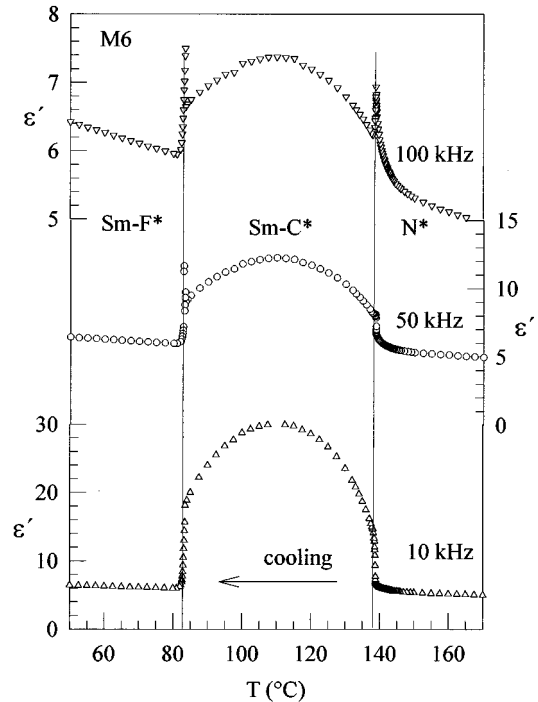

FIG. 4. Dielectric constant ε' versus temperature for compound $M6$ at frequencies of 100 kHz, 50 kHz, and 10 kHz in the ''planar orientation.'' The peaks indicating the phase transitions are hidden on lowering the frequency.

ing the N^*–Sm-C^* phase transition on cooling and represent a distinct peak at the N^*–Sm-C^* phase transition. The action of an electric field or hydrodynamic flow induced by a displacement of ionic charges negligibly effects the structure of the N^* phase since the magnitude of the electric field is small and its period is at least a hundred times shorter than the characteristic time describing the transport of ionic impurities across the cell. However, the formation of smectic clusters connected to an increase of the cholesteric pitch in the vicinity of the N^*–Sm-C^* phase transition may cause an increase of the dielectric constant, which might be related to the linear electroclinic effect of the chiral nematic phase near a transition into a smectic phase [32,33]. Similar to the electroclinic effect in chiral smectic phases, a tilt of the optical axis was established by electro-optical measurements in the chiral nematic phase of infinite or sufficiently large pitch [34]. Further dielectric measurements in the high frequency region ($f > 100$ kHz) are required to characterize the corresponding dielectric mode with respect to its dielectric increment and relaxation time.

Within the Sm-C^* phase, the values of ε' linearly increase with decreasing temperature. The slope remains almost unchanged after passing the Sm-F^* phase transition. The overall increase of ε' on lowering temperature can be associated with an increase of volume density of compound $M6$. A distinct peak in the curve of ε' versus temperature indicates the Sm-C^*–Sm-F^* phase transition as shown in Figs. 3 and 4.

The permittivity is reproduced within instrumental error. On heating the same sample starting in the Sm-F^* phase the same values are obtained as on cooling (cf. Fig. 3), but within the Sm-C^* phase, the values of ε' are significantly larger in comparison to those obtained in the preceding cooling process. The larger dielectric constants obtained for the heating process relax to the smaller values measured on cooling after the system is kept overnight at a temperature of $100\,^{\circ}$C. This process is related to a structural change in the sample. Simultaneously performed texture observations indi-

cate a modification of the spatial director structure for this process: Equally spaced disclination lines indicate the presence of a distorted Sm-C^* helicoidal structure, which is observed in the Sm-C^* phase in a slow cooling process, whereas these disclination lines are absent in the Sm-F^* phase, and they remain absent after the cell is heated to the Sm-C^* phase again. The disclination lines return after the spatial director structure relaxes overnight. These texture observations and dielectric measurements suggest that the helical structure of the Sm-F^* phase is absent in compound $M6$ prepared in this SSFLC cell. Generally, it cannot be concluded that the Sm-F^* phase is not helical [36], but the bond orientational order, surface, and elastic interactions might suppress the formation of a helicoidal structure or its helical pitch exceeds the sample dimensions. However, in the Sm-C^* phase, the dielectric constants obtained on heating are related to a splayed state, whereas the values of ε'(200 kHz) measured on cooling are connected to a distorted helicoidal structure. Since the former values are larger than the latter, compound $M6$ exhibits a negative dielectric anisotropy in the Sm-C^* phase, if the dielectric biaxiality of the phase is neglected.

Figure 4 depicts the dielectric permittivity $\varepsilon'(T)$ measured at lower frequencies. Unlike in the Sm-C^* phase, $\varepsilon'(T)$ is almost independent of frequency in a range between 10 kHz and 200 kHz, in both the N^* and Sm-F^* phases. At a fixed temperature, the strong collective director mode due to a small reorientation of the $\vec{c}$ director in the Sm-C^* phase causes an increase of dielectric constant ε' with decreasing frequency. The peaks related to phase transitions are hidden on lowering the frequency as can be noticed from the lower
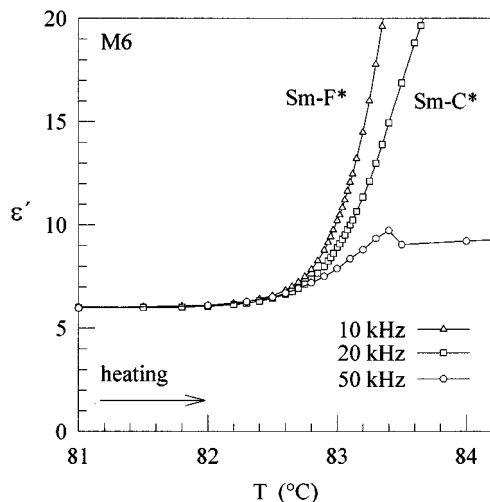
FIG. 5. The dielectric constant ε' versus temperature upon heating for compound $M6$ (''planar orientation'') in the vicinity of the Sm-F^*–Sm-C^* phase transition at frequencies of 10 kHz, 20 kHz, and 50 kHz in the absence of a bias electric field.

FIG. 6. Comparison of the dielectric and optical responses obtained in cells stabilizing a ''planar orientation'' and filled with compound $M6$. Both signals are simultaneously measured at a frequency of 10 kHz on heating (same cell as used in Fig. 5).

panel of Fig. 4. It should be mentioned that the mobility of ionic impurities affects the dielectric measurements for frequencies lower than 100 Hz and the resistance capacitance (RC) relaxation of ITO electrodes influences the spectra for frequencies exceeding 300 kHz. Substantial work on dielectric properties of the Sm-C^* phase has been performed [37]. However, phase transitions into hexatic smectic phases have scarcely been studied and have gained our interest.

A. Sm-F^*–Sm-C^* phase transition

In compound $M6$ the strong mode related to collective order parameter reorientations in the Sm-C^* phase overlaps with processes connected to the Sm-F^*–Sm-C^* phase transition as can be deduced from Fig. 5, which shows a continuous increase of the dielectric constant ε' with increasing temperature in the vicinity of this phase transition for frequencies lower than 50 kHz.

If a cell is mounted in a polarizing microscope and its position is optimized with respect to the modulation depth of the light intensity (546 nm), the dielectric permittivity ε'(10 kHz) and the optical signal can be simultaneously measured on heating. The results are compared in Fig. 6. In a heating process, the modulation depth of the optical signal increases similar to the dielectric permittivity ε', thus both methods provide equal information here. With increasing temperature, both the hexagonal order parameter and the coupling between local tilt to bond directions decrease, thus dielectric increments of collective director modes related to a reorientation of the $\vec{c}$ director rise in the vicinity of a Sm-F^*–Sm-C^* phase transition.

The application of a bias electric field is appropriate to suppress collective director modes in the Sm-C^* phase [38]. Figure 7 depicts the dielectric constant ε' in the same temperature region as in Fig. 6 with a dc bias electric field applied. Unlike in the absence of the bias electric field, the peak associated with the Sm-F^*–Sm-C^* phase transition can clearly be observed down to a frequency of 10 kHz. This
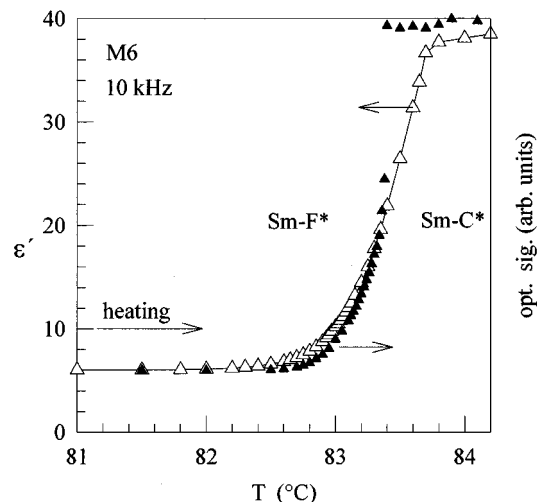
behavior supports the general assumption that the application of a bias electric field suppresses the strong mode related to the Sm-C^* phase more significantly than processes associated to the Sm-F^*–Sm-C^* phase transition.

The optical method has an important advantage [35]: The direction of the electric field applied can be chosen independently of the direction of light propagation, for instance, perpendicular to each other for the ''homeotropic orientation'' (cf. Fig. 1). In the vicinity of the Sm-F^*–Sm-C^* phase transition of compound $M6$, the modulation depth of the light intensity (546 nm) is measured as a function of frequency and temperature in ''homeotropic orientation'' and depicted in Fig. 8. Even in the absence of a bias electric field, the peak associated with the phase transition is clearly revealed in a frequency range between 10 Hz and 50 kHz. This mode exhibits a relaxation frequency of approximately 3 kHz. It van-
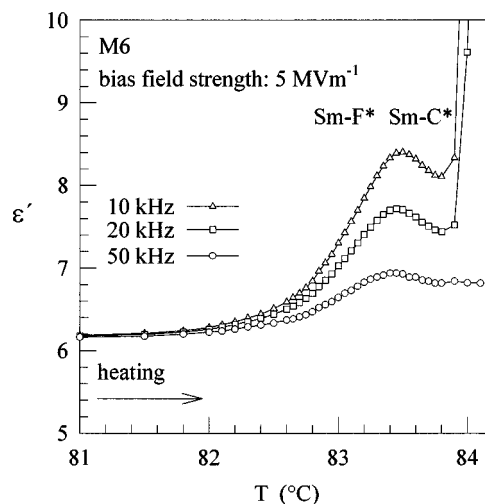

FIG. 7. The dielectric constant ε' versus temperature for compound $M6$ (''planar orientation'') in the vicinity of the Sm-F^*–Sm-C^* phase transitions on heating at frequencies of 10 kHz, 20 kHz, and 50 kHz and a bias electric field of 5MV m^{-1} applied.
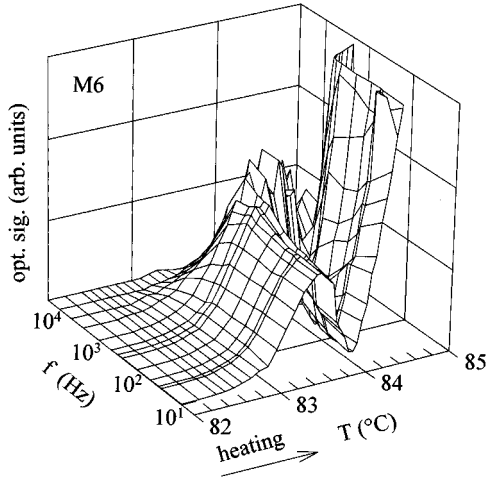
FIG. 8. The modulation depth of the light intensity for compound $M6$ (''homeotropic orientation'') as a function of frequency and temperature in the vicinity of the Sm-F^*–Sm-C^* phase transition on heating. No bias electric field applied.

FIG. 9. Structure of a homogeneous slab of a chiral hexatic Sm-F^* phase. (X,Y,Z) is the laboratory coordinate system, $\vec{z}$ smectic layer normal, $\vec{P}_s$ spontaneous polarization, $\vec{c}$ unit vector describing the local tilt direction, and $\vec{E}$ electric field along $\vec{x}$. The hexagon symbolizes the long ranged bond orientational order within the $\vec{x}$, $\vec{y}$ plane, but a long ranged positional order is absent within the smectic layers. In principle, an electric field induced reorientation of the tilt direction is divided into two contributions: (i) A reorientation of the bond orientational order (hexagon) with the local tilt direction locked to the hexagon and (ii) a reorientation of the local tilt direction with respect to the bond orientational order being spatially fixed to the cell walls. The substrates of the samples are normal to the $\vec{x}$ direction (''planar'') or normal to the $\vec{z}$ direction (''homeotropic'').

ishes 1 K above the Sm-F^*–Sm-C^* phase transition, which occurs at 83 °C. Within the Sm-C^* phase a rapid increase of the modulation depth is detected for frequencies smaller than 10 kHz.

Far below the Sm-F^*–Sm-C^* phase transition, the bond orientational order is assumed to be long ranged and spatially fixed with respect to the cell walls. If the coupling between the bond orientational order and the local tilt direction is strong additionally, both the $\vec{c}$ director and the spontaneous polarization are locked. Collective director modes connected to order parameter phase changes are small.

On approaching the Sm-F^*–Sm-C^* phase transition on heating, the coupling between the bond orientational order and the local tilt direction becomes weak, thus allowing a reorientation of the $\vec{c}$ director with respect to the bond orientational order, which remains long ranged and spatially fixed. This process might be associated with the peak directly indicating the Sm-F^*–Sm-C^* phase transition, which is detected in the dielectric (''planar'' orientation) and the optical signal (''planar'' or ''homeotropic'' orientation) at different frequencies, respectively. On further heating, the correlation length of the bond orientational order also decreases, thus allowing small pertubations of the spatial director configuration of the LC cell. In the Sm-C^* phase, the bond orientational order is short ranged and comparatively weak elastic and surface interactions couple the local tilt direction with respect to the cell walls.

These experimental results may be explained in terms of a collective reorientation of the $\vec{c}$ director in hexatic smectic phases, which are influenced by the coupling between the spontaneous polarization and the electric field. This induced process can be divided into two contributions depicted in Fig. 9:

(i) The local tilt direction ($\vec{c}$ director) and the direction of the bond orientational order (hexagons) are fixed with respect to each other, if the coupling between both is assumed to be infinitely strong. In this limit, any rotation of the spontaneous polarization requires a rotation of local bonds. Since
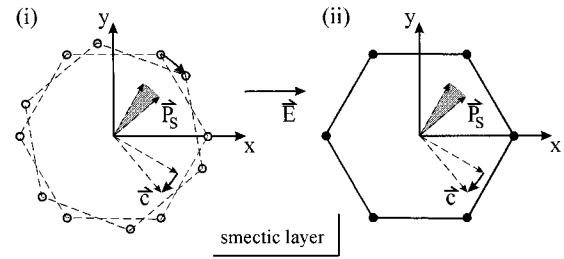
three dimensional long range positional order is absent in hexatic phases, this process is different from a rotation of the sample.

(ii) If the bond orientational order is assumed to be spatially fixed with respect to the cell walls, any rotation of the spontaneous polarization is affected by the coupling between the local tilt direction and the bond orientational order. In this limiting case, the $\vec{c}$ director must leave its equilibrium direction at zero electric field, which points towards the apex of the hexagon in a Sm-I^* phase and towards the side of the hexagon in a Sm-F^* phase, respectively.

Contribution of collective director phase fluctuations (reorientations of the $\vec{c}$ director) to the complex dielectric permittivity in tilted smectic phases are designated a ''Goldstone mode.'' This deviates from its original definition [39], which describes a zero-frequency, symmetry restoring, and ''gapless'' mode. In a dielectric experiment, such a mode is undetectable in a chiral tilted smectic phase either in a helical or in a surface stabilized director configuration [40], because it requires a small, but energy consuming perturbation of the spatial director configuration against elastic and surface interactions [41]. In some chiral tilted smectic phases the tilt direction is intrinsically locked in a certain position on the local tilt cone, e.g., in antiferroelectric phases or in hexatic phases. This paper deals with the latter case. Since forces stabilizing the tilt direction can be large in comparison to weak elastic and surface interactions, the term ''Goldstone mode'' becomes unsuitable here.

B. Sm-F^*–Sm-I^* phase transition

Homologues of the series Mn exhibit a monotropic Sm-F^* and Sm-I^* phase, if the alkoxy chain contains more than six carbon atoms. Compound $M10$ with its chemical structure and phase sequence given below is used for further in-
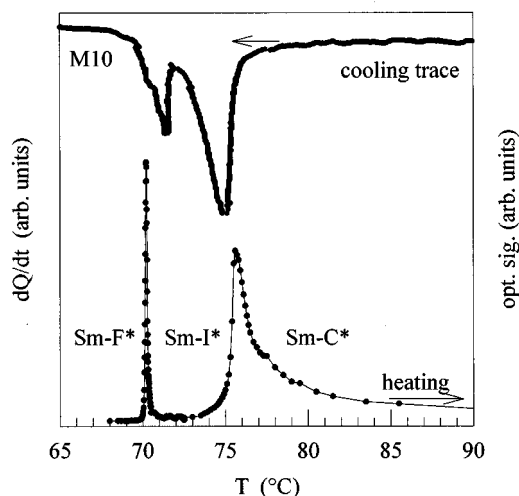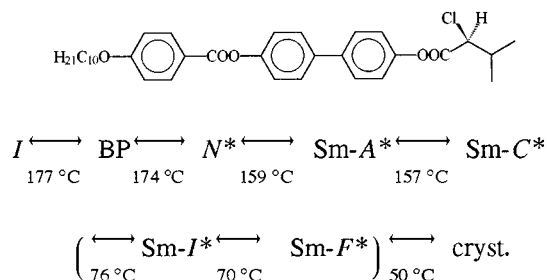
FIG. 10. Comparison of a DSC cooling trace of compound *M*10 with measurements of the modulation depth of the light intensity obtained in ''homeotropic orientation'' without a bias electric field applied. Phase transitions from and to hexatic phases are properly detected by both methods.

vestigations:

$$I \xleftrightarrow[177\,°C]{} BP \xleftrightarrow[174\,°C]{} N^* \xleftrightarrow[159\,°C]{} Sm\text{-}A^* \xleftrightarrow[157\,°C]{} Sm\text{-}C^*$$

$$\left(\xleftrightarrow[76\,°C]{} Sm\text{-}I^* \xleftrightarrow[70\,°C]{} Sm\text{-}F^* \right) \xleftrightarrow[50\,°C]{} cryst.$$

In the vicinity of a Sm-F^*–Sm-I^* phase transition, the local tilt direction changes its position with respect to the bond orientational order: In the Sm-F^* phase molecules are tilted towards their next-nearest neighbors whereas molecules are tilted towards their next neighbors in the Sm-I^* phase. The modulation depth of the light intensity for a sample of compound $M10$ is measured in ''homeotropic orientation'' and the results are depicted in Fig. 10 along with a differential scanning calorimetry (DSC) trace (Perkin-Elmer DSC 7, mass 4.7 mg, cooling rate -5 K min^{-1}). The optical method is sensitive to the Sm-F^*–Sm-I^* and the Sm-I^*–Sm-C^* first order phase transitions as can be concluded from a comparison of both curves.

The bond orientational order is assumed to be unaffected in the vicinity of the hexatic-to-hexatic phase transition. With Φ being the angle between the local tilt direction and the bond orientational order (see Fig. 11) the part of the free energy density function f describing the tilt-to-bond coupling can be expanded in a Fourier series due to the local pseudohexagonal symmetry formed by the center of mass of molecules [24] in the vicinity of the Sm-F^*–Sm-I^* phase transition

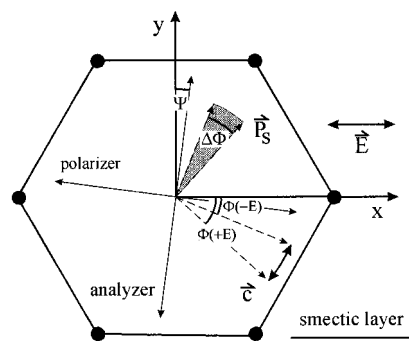$$f(\Phi) = -\sum_{n=1}^{\infty} \frac{1}{6n} a_n \cos(6n\Phi). \quad (1)$$

FIG. 11. Variables used for a description of the coupling between the bond orientational order and the local tilt direction in the vicinity of the Sm-F^*–Sm-I^* phase transition.

(Due to the tilt of molecules, symmetry of a single smectic layer is C_2. Hence, a nonzero, local spontaneous polarization is built up.) Selinger and Nelson pointed out that the coefficients a_n decrease rapidly with increasing n, therefore the Fourier series might be truncated after the second term. The Sm-F^*–Sm-I^* phase transition can be described with a fixed $a_2 > 0$ and a temperature dependent coefficient $a_1 = \alpha(T - T_c)$, which changes sign at the phase transition temperature T_c. In the absence of an electric field E, the free energy density $f(\Phi, T)$ reads

$$f(\Phi, T) = -\frac{1}{6}\alpha(T - T_c)\cos(6\Phi) - \frac{1}{12}a_2\cos(12\Phi). \quad (2)$$

In the vicinity of the Sm-F^*–Sm-I^* phase transition, a spontaneous polarization of 210 nC cm^{-2} has been measured for $M10$ [28]. Since $\vec{P_s}$, the layer normal $\hat{z}$, and the director $\hat{n}$ form a right-handed system in compounds Mn, a negative term $-P_s E \cos[\Phi + (\pi/2)]$ must be added to $f(\Phi, T)$ in the presence of an electric field E,

$$f(\Phi, T, E) = f_0 - \frac{1}{6}\alpha(T - T_c)\cos(6\Phi) - \frac{1}{12}a_2\cos(12\Phi)$$
$$- P_s E \cos\left(\Phi + \frac{\pi}{2}\right). \quad (3)$$

Minimization with respect to Φ leads to

$$\frac{\partial}{\partial \Phi} f(\Phi, E, T) = \alpha(T - T_c)\sin(6\Phi) + a_2\sin(12\Phi)$$
$$+ P_s E \cos(\Phi)$$
$$= 0. \quad (4)$$

The thermal equilibrium values $\Phi_0(E, T)$ are calculated as a function of temperature and electric field strength using the computer program MAPLE V for solving Eq. (4) numerically. In the vicinity of the Sm-F^*–Sm-I^* phase transition, calculated values of $\Phi_0(E, T)$ are displayed in Fig. 12. Sign inversion of the electric field applied induces a reorientation of the local tilt direction with respect to the spatially fixed long ranged bond orientational order of a magnitude $\Delta\Phi_0(T, E) = |\Phi_0(T, -E) - \Phi_0(T, E)|$, which is plotted in
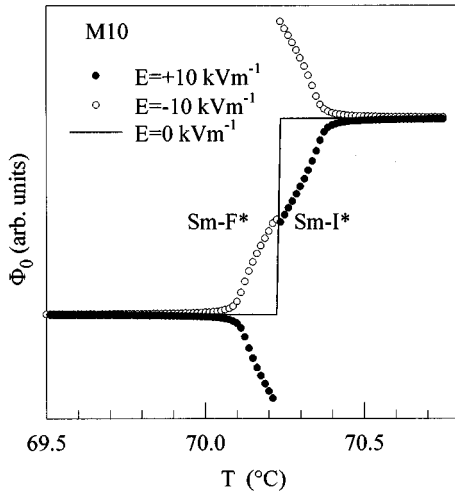
FIG. 12. Calculated values of the azimuthal angle Φ_0 as a function of temperature for different electric field strengths. The following parameters are used for calculations: $P_sE=21$ J m^{-3}, $\alpha=4.2$ J K^{-1} m^{-3}, $a_2=0.22$ J m^{-3}.

Fig. 13. The width of the peak indicating the Sm-F^*–Sm-I^* phase transition is significantly influenced by the ratio α/a_2. This reorientation changes the transmission $\Delta I(T,E)$ of the cell,

$$\Delta I(T,E) \sim \sin^2\{2[\Psi+\Phi_0(T,-E)]\} - \sin^2\{2[\Psi+\Phi_0(T,E)]\}. \quad (5)$$

The angle Ψ describes the position of the cell with respect to the polarizers (see Fig. 11). During the experiments, Ψ is fixed to maximize ΔI in the Sm-F^* phase [$\Psi=-(\pi/24)$]. The calculated change of transmission ΔI is depicted in Fig. 14 and compared to the modulation depth of the light intensity. The width of both peaks is similar, from which the ratio α/a_2 is determined to be 19 K^{-1}.

Unlike for the measurement conditions, the calculations refer to a ''static'' experiment, with the system in a thermal equilibrium state. Nevertheless, ''dynamic'' measurements
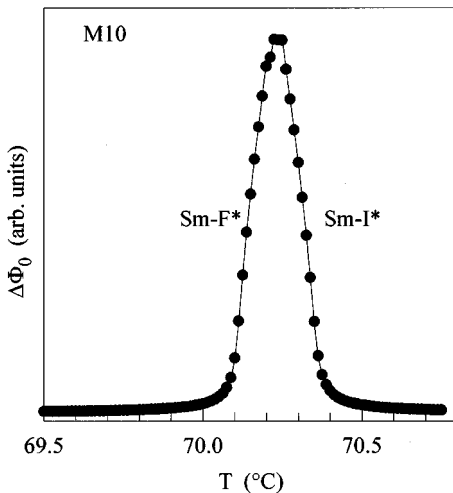

FIG. 13. Electric field induced reorientation $\Phi_0(T,E)$ of the azimuthal angle with respect to a spatially fixed bond direction.
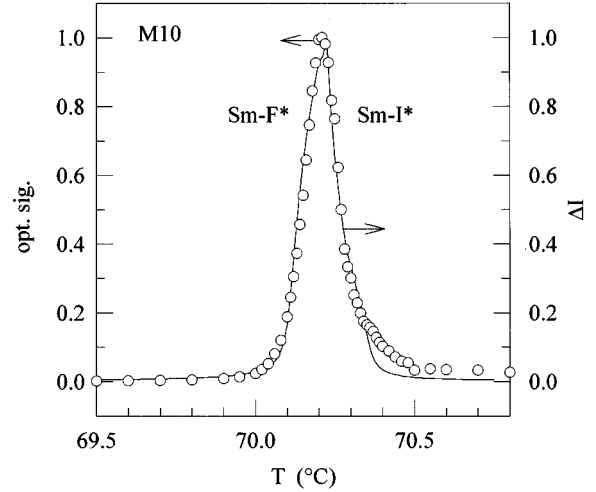

FIG. 14. Change of transmission of the cell ΔI calculated with Eq. (5) using values from Fig. 12. For comparison, the modulation depth of the light intensity at 110 Hz and amplitude of the electric field of 10 kV m^{-1} is displayed.

have been performed with an oscillating electric field $E=E_0\sin(\omega t)$ with a frequency of $f=110$ Hz, because at lower frequencies ionic impurities will affect the measurements. Therefore Φ is a function of space and time and it is the solution of a differential equation of motion describing a reorientation of the local tilt direction with respect to the bond orientational order. This differential equation will include the tilt-to-bond coupling $f(\Phi,T,E)$ and additional contributions due to viscose, elastic, and surface interactions, that have been neglected in a first approximation. If Φ becomes large, the solution of this equation of motion involves nonlinear contributions, which are not detected by the lock-in technique. The distribution of tilt directions with respect to the direction of mechanical shear is neglected for simplicity, and the liquid crystal is assumed to act as a homogeneous slab. Furthermore, any reorientation of the bond orientational order in space or time is neglected. For these reasons, absolute values of calculated and measured ΔI can hardly be compared to extract absolute values of α and a_2. Therefore measurements of Φ as a function of frequency and amplitude of the oscillating electric field are required.

The influence of the cell thickness is another interesting topic. We have chosen a cell thickness of approximately 1 μm in order to achieve a nearly uniform director structure by shearing. If the cell thickness increases, a nonuniform or modified helical director structure might be formed in some tilted hexatic phases. This will affect the collective director modes in hexatic liquid crystalline phases. Further work concerning the dynamics of the $\vec{c}$ director in hexatic phases is in preparation and it will provide additional information on the nature of hexatic-to-hexatic phase transitions.

IV. CONCLUSIONS

Collective director modes in chiral, liquid crystalline materials reflect smectic-to-cholesteric, hexatic-to-Sm-C^*, or hexatic-to-hexatic phase transitions in the homologous series Mn. For detection of these modes related to pertubations of the spatial director configuration, dielectric and electro-

optical measurements are applied and equivalent information is provided by both methods. Collective director reorientations in the vicinity of the Sm-*F**–Sm-*C** phase transition are influenced by the temperature dependent hexagonal ordering (long ranged bond orientational order) and its coupling to the local direction of molecular tilt ($\vec{c}$ director). In principle, a reorientation of the $\vec{c}$ director in hexatic tilted phases can be divided into two mechanisms.

(i) With the local tilt direction ($\vec{c}$ director) strictly coupled to the direction of the bond orientational order, a rotation of the $\vec{c}$ director requires a rotation of local bonds with respect to cell walls.

(ii) With the bond orientational order being spatially fixed with respect to the cell walls, a rotation of the $\vec{c}$ director affects the coupling between the local tilt direction and the bond orientational order.

Both mechanisms are observed in the vicinity of the Sm-*F**–Sm-*C** phase transition in compound *M*6. In the vicinity of the hexatic-to-hexatic phase transition (Sm-*F**–Sm-*I**), the coupling between the bond orientational order and the local tilt direction becomes weak. By adding the ferroelectric interaction to the free energy density of the sample, the electric field induced reorientations of the $\vec{c}$ director can be calculated as a function of temperature and electric field strength. Reduced coefficients proposed by Selinger and Nelson can be deduced from fitting the measurements to the calculated data.

[1] L. D. Landau, Phys. Z. Sowjetunion **11,** 26 (1937); Zh. Eksp. Teor. Fiz. **7**, 19 (1937).

[2] R. E. Peierls, Helv. Phys. Acta **7**, 81 Suppl. II (1934); Ann. Inst. Henri Poincare **5**, 177 (1935).

[3] L. D. Landau, Phys. Z. Sowjetunion **11**, 545 (1937); Zh. Eksp. Teor. Fiz. **7**, 627 (1937).

[4] J. D. Brock, R. J. Birgeneau, J. D. Litster, and A. Aharony, Phys. Today **7**, 52 (1989).

[5] J. D. Brock, D. Y. Noh, B. R. McClain, J. D. Litster, R. J. Birgeneau, A. Aharony, P. M. Horn, and J. C. Liang, Z. Phys. B **74**, 197 (1989).

[6] R. B. Meyer, L. Lièbert, L. Strzelecki, and P. Keller, J. Phys. (France) Lett. **36**, L-69 (1975).

[7] N. A. Clark and S. T. Lagerwall, Appl. Phys. Lett. **36**, 899 (1980).

[8] J. Doucet, P. Keller, A. M. Levelut, and P. Porquet, J. Phys. (France) **39**, 548 (1978).

[9] A. J. Leadbetter, J. P. Gaughan, B. Kelly, G. W. Gray, and J. W. Goodby, J. Phys. (France) Colloq. **40**, C3-178 (1979).

[10] A. J. Leadbetter, J. Frost, J. P. Gaughan, and M. A. Mazid, J. Phys. (France) Colloq. **40**, C3-185 (1979).

[11] P. A. C. Gane, A. J. Leadbetter, and P. G. Wrighton, Mol. Cryst. Liq. Cryst. **66**, 247 (1981).

[12] C. C. Huang, G. Nounesis, R. Geer, J. W. Goodby, and D. Guillon, Phys. Rev. A **39**, 3741 (1989).

[13] G. Nounesis and C. C. Huang, Phys. Rev. Lett. **56**, 1712 (1986).

[14] J. M. Viner and C. C. Huang, Phys. Rev. A **27**, 2763 (1983).

[15] S. C. Lien, J. M. Viner, C. C. Huang, and N. A. Clark, Mol. Cryst. Liq. Cryst. **100**, 145 (1983).

[16] G. Nounesis, R. Geer, H. Y. Liu, C. C. Huang, and J. W. Goodby, Phys. Rev. A **40**, 5468 (1989).

[17] T. Stoebe, R. Geer, C. C. Huang, and J. W. Goodby, Phys. Rev. Lett. **69**, 2090 (1992).

[18] S. B. Dierker and R. Pindak, Phys. Rev. Lett. **59,** 1002 (1987).

[19] S. Sprunt and J. D. Litster, Phys. Rev. Lett. **59**, 2682 (1987).

[20] S. Sprunt, M. S. Spector, and J. D. Litster, Phys. Rev. A **45**, 7355 (1992).

[21] M. S. Spector, S. Sprunt, and J. D. Litster, Phys. Rev. E **47**, 1101 (1993).

[22] M. S. Spector and J. D. Litster, Phys. Rev. E **51**, 4698 (1995).

[23] D. R. Nelson and B. I. Halperin, Phys. Rev. B **21**, 5312 (1980).

[24] J. V. Selinger and D. R. Nelson, Phys. Rev. Lett. **61**, 416 (1988).

[25] J. V. Selinger and D. R. Nelson, Phys. Rev. A **39**, 3135 (1989).

[26] R. J. Cava, J. S. Patel, and E. A. Rietman, J. Appl. Phys. **60**, 3093 (1986).

[27] K. Mohr, S. Köhler, K. Worm, G. Pelzl, S. Diele, H. Zaschke, D. Demus, G. Andersson, I. Dahl, S. T. Lagerwall, K. Skarp, and B. Stebler, Mol. Cryst. Liq. Cryst. **146**, 151 (1987).

[28] J. Schacht, I. Dierking, F. Gießelmann, K. Mohr, H. Zaschke, W. Kuczyński, and P. Zugenmaier, Liq. Cryst. **19**, 151 (1995).

[29] F. Grandjean, C. R. Acad. Sci. **172**, 71 (1921).

[30] H. Takezoe, Y. Ouchi, K. Ishikawa, and A. Fukuda, Mol. Cryst. Liq. Cryst. **139**, 27 (1986).

[31] T. P. Rieker, N. A. Clark, G. S. Smith, D. S. Parmar, E. B. Sirota, and C. R. Safinya, Phys. Rev. Lett. **59**, 2658 (1987).

[32] L. Zili, R. G. Petschek, and C. Rosenblatt, Phys. Rev. Lett. **62,** 796 (1989).

[33] K. A. Crandall, S. Tripathi, and C. Rosenblatt, Phys. Rev. A **46**, R715 (1992).

[34] L. Komitov, S. T. Lagerwall, B. Stebler, G. Andersson, and K. Flatischler, Ferroelectrics **114**, 167 (1991).

[35] W. Kuczyński, J. Hoffmann, and J. Małecki, Ferroelectrics **150**, 279 (1993).

[36] W. Kuczyński and H. Stegemeyer, Liq. Cryst. **5**, 553 (1989).

[37] L. M. Beresnev, L. M. Blinov, and E. B. Sokolova, Pis'ma Zh. Éksp. Teor. Fiz. **28**, 340 (1978) [JETP Lett. **28**, 317 (1978)].

[38] J. Pavel and M. Glogarová, Ferroelectrics **121**, 45 (1991).

[39] J. Goldstone, A. Salam, and S. Weinberg, Phys. Rev. **127**, 965 (1962).

[40] I. Muševič, B. Žekš, and R. Blinc, Phys. Rev. B **49**, 9299 (1994).

[41] J. Schacht, F. Gießelmann, P. Zugenmaier, and W. Kuczyński, Ferroelectrics **173**, 157 (1995).